Analog Integr Circ Sig Process (2015) 82:99–111
DOI 10.1007/s10470-014-0446-2

Design and implementation of a wireless medical system prototype for implantable applications

Jesus Efrain Gaxiola-Sosa · Kamran Entesari

Received: 31 October 2013 / Revised: 6 May 2014 / Accepted: 12 November 2014 / Published online: 28 December 2014

Abstract The design, implementation and testing of a wireless medical system (WMS) for continuous monitoring of biological parameters are presented in this paper. Special emphasis has been made on the implantable unit prototype. The proposed system consists of three main sections: implantable medical device (IMD), base station (BS) and graphical user interface. The IMD and BS communicate through an RF link that operates in both the industrial, scientific and medical (ISM, at 2.4–2.48 GHz) and the medical implantable communication service (MICS, at 402–405 MHz) bands. The IMD and BS are based on two commercially-available ultra-low power integrated circuits: a mixed-signal microcontroller and a medical implantable radio transceiver. A comprehensive explanation of the main design issues and implementation challenges is presented. The details regarding the analog front-end functionality, a low-power-oriented algorithm, an analysis of power consumption versus lifetime and a customized operating mode for power optimization are explained. The main considerations for link budget calculations in implantable applications are discussed. A test bench designed to emulate real conditions is used to verify the functionality of the WMS showing successful communication up to 2.1 m range with a data rate of 200 Kbps. The IMD works from a 3 V power supply with an average current consumption of 0.572 mA (including RF transmission) in continuous operation. This allows a 2 year IMD lifetime in periodic operation (for a 350 mAh battery), delivering 1 h of information per day.

Keywords Implantable device · MICS band · Low-power · Wireless medical system

1 Introduction

Advances in medical technology have allowed physicians to improve the patients' quality of life through the use of wireless medical systems (WMS) aimed to provide reliable monitoring and high accuracy diagnostics [1]. A typical WMS includes an end device (ED) and a base station (BS) complemented by a graphical user interface (GUI) implemented in a computer [2]. The ED is in charge of collecting information about a specific physiological or biochemical parameter while the BS acts as a gateway between the ED and the GUI. Depending on the application, the ED can be wearable (non-invasive) or implantable (invasive) and the WMS can be targeted to complement the patient's treatment or as part of a research study.

The main issues related with the implementation of such systems are size, cost and lifetime, especially when the monitoring unit is an implantable medical device (IMD) [3]. Key solutions to these issues are the selection of the right hardware (including battery) along with the use of a smart software control algorithm to optimize the power consumption. In terms of hardware, designers have three main options to choose from: application specific integrated circuits (ASICs), programmable systems on chip (PSoCs) and off-the-shelf components. ASICs offer the highest level of innovation, small size and the best power performance. However, their design implies high cost and long development periods. Programmable SoCs provide some design

J. E. Gaxiola-Sosa (✉)
IoT Home Products, Silicon Labs Inc, 200 W Cesar Chavez St, Austin, TX 78701, USA
e-mail: efgaxiol@silabs.com

K. Entesari
Department of Electrical and Computer Engineering, Analog and Mixed-Signal Center, Texas A&M University, 315A WERC, TAMU 3128, College Station, TX 77840, USA

flexibility, modest cost and relatively fast implementation. Nevertheless, power optimization is limited to the performance of each individual block. Finally, the use of commercial ICs allows fast prototyping while keeping a low price, but the size and power consumption of the system become restricted by the characteristics of the chosen components. Regarding the software, power optimization can be achieved by using only a microprocessor core in ASICs and PSoCs instead of a complete microcontroller (MCU), as in the off-the-shelf case. Taking this into consideration, careful analysis of the application, available resources and time restrictions should be done in order to determine the optimum way to implement the WMS.

This work presents a WMS prototype intended for implantable applications. The implantable unit design takes advantage of the qualities of the three hardware options mentioned before while minimizing the cons that come along with each of them, resulting in a fully programmable system-on-board. The presented BS allows power optimization of the IMD radio through the use of two different radio bands for wake-up and data transmission.

The aim of the system is to monitor the blood pressure of laboratory animals for drug safety research. However, the approach employed in this study can be used to implement an IMD targeted to monitor other physiological or biochemical parameters such as pH, temperature, phosphorus-based blood gases, etc. Moreover, the WMS includes the option of modifying the signal resolution and frequency of data collection according to the specific needs of the user. The paper organization is as following: Sect. 2 discusses the WMS design and implementation, Sect. 3 shows the software control algorithm, Sect. 4 presents a power versus lifetime analysis based on the amount of data collected by the IMD, Sect. 5 shows experimental results and Sect. 6 concludes the paper.

2 System design and implementation

A block diagram of the WMS, including simplified versions of the IMD and the BS, is presented in Fig. 1. Both

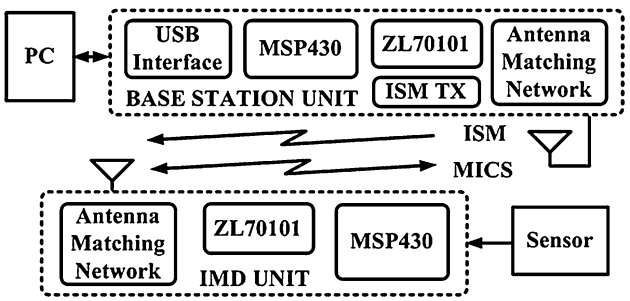

Fig. 1 Block diagram of the WMS

units are based on two off-the-shelf integrated circuits (ICs) intended for ultra-low-power applications: the Texas Instruments MSP430FG4618 [4], a mixed-signal MCU; and the Microsemi (formerly Zarlink) ZL70101 [5], a medical implantable radio transceiver. The MCU enables the design of a low-power-oriented control algorithm through its capability of shutting down peripherals that are not used at know time intervals. This provides PSoC characteristics to the IMD in the sense of power performance. The transceiver is an ASIC that operates at the medical implant communication service (MICS) band at 402–405 MHz to send/receive biological information/instruction-commands to/from the BS unit and includes an on-chip ultra-low power wake-up mechanism operating in the industrial, scientific and medical (ISM) band at 2.45 GHz to listen for a wake-up signal from the BS unit. The media access controller (MAC) of the transmitter allows it to operate as an extra MCU peripheral, enabling the integration of a system-on-board capable of supporting a software control algorithm to optimize the overall power consumption of the IMD.

The basic operation principle of the WMS can be summarized as follows: the BS transmits a wake-up signal to the IMD using the ISM band and the IMD replies with an acknowledge message using the MICS band. Once the link is established, further communications are handled using the MICS band. This frequency band is regulated by the Federal Communications Commission (FCC) for implantable biotelemetry applications [6] and was allocated at 402–405 MHz due to the signal propagation characteristics in the human body (at this frequency, the attenuation of the RF signal is smaller in comparison with other bands). Moreover, although continuous implantable communication at 2.45 GHz is possible, this would be translated into higher power consumption on the transceiver. After a given number of physiological measurements is stored in the IMD, the collected data is sent to the BS which in turn, will transmit it to the PC via universal serial bus (USB) connection. Once in the computer, the GUI allows the user to view the information in real-time and stores the samples in text files available for future analysis. A discussion on the battery selection, along with a detailed description of the IMD and the BS units are presented in the next subsections.

2.1 Battery selection

IMD batteries differ from regular batteries because [7]: (1) they operate in an isothermal environment (constant temperature of 37 °C), (2) they need to be replaced prior total battery depletion, requiring surgical intervention, (3) their size and form dominate the IMD's volume and shape, and (4) their current capacity dictates the IMD lifetime.

Therefore, the battery constitutes a critical part in the design of an IMD.

Several options were explored in order to select the battery for the presented IMD, including different lithium-based options (Li/I_2, $Li/SOCl_2$, $LiNiCoAlO_2$) from providers such as Greatbatch Inc., Quallion LLC, and Eagle Picher Medical Power™. The nominal voltage, volume in cubic centimeters (1 cc = 1 cm^3), battery capacity in mili ampere per hour (mAh) and chemistry are shown in Table 1. Based on the, trade-off between battery size and power, and taking into account a peak current drain >6 mA (in RF transmission mode), a $Li/SOCl_2$ battery from Eagle Picher with a capacity of 350 mAh, prismatic shape, and total volume of 1.66 cc [8], is chosen to be the reference battery for the proposed IMD.

2.2 Implantable medical device

The most critical section of the presented system is the IMD. A detailed block diagram describing its main components is presented in Fig. 2, including a MCU, a wireless transceiver, a dual-band matching network and a few external components such as bypass capacitors, crystal oscillators and resistors as part of the analog front-end (AFE). The IMD is powered by an external battery which is periodically monitored by the supply voltage supervisor (SVS) peripheral, included in the MCU.

2.2.1 Signal acquisition and analog to digital conversion

A sensor translates the physiological parameter into an electrical signal. The signal is injected into instrumentation amplifier (IA) built using the MCU's on-chip op amps and external passive components. The MCU has the ability to turn the op amps off when they are not being used, in order to reduce the power consumption of the IMD. A three op amp IA topology including an antialiasing filter is selected as the IMD's AFE and its schematic diagram is presented in Fig. 3. This IA implementation rejects electromagnetic and electrostatic interferences with a common-mode rejection ratio (CMRR) better than 80 dB [9–11]. The first stage of the IA is composed of two op amps in non-inverting configuration in order to provide high input impedance to the incoming differential signal. The second stage is configured as a difference amplifier [12] and includes an antialiasing filter to remove out of band interferences whose folding after the analog to digital conversion would corrupt the signal band [13]. The gain bandwidth product, power consumption and CMRR of the op amps are 500 kHz, 60 μA 70 dB, respectively [4]. The gain and cut-off frequency of the IA are given by Eqs. (1) and (2). The external passive components used on the IA are: R1(variable) = 0–250 KΩ, R2 = 1 MΩ, R3 = 200 KΩ, R4 = 10 MΩ and C = 1nF.

$$V_{OUT} = (V_{IN+} - V_{IN-})\left(1 + \frac{2 \cdot R2}{R1}\right)\left(\frac{R4}{R3}\right) \quad (1)$$

$$f_{3dB} = \frac{1}{2\pi \cdot R4 \cdot C} \quad (2)$$

The output of the IA is connected to a 12-bit successive approximation register analog to digital converter (SAR-ADC), also included as part of the MCU. This module can be shut down after a conversion is completed and includes a buffer where the samples are stored before being sent to the random access memory (RAM) [4]. Since most physiological signals have similar bandwidths (from DC up to 250 Hz) [14, 15] and because of the low power features of the SAR-ADC topology [13], it is possible to modify the ADC's oversampling ratio (OSR) up to 30 in order to increase the accuracy of the conversion without compromising the power consumption. Having this relatively high OSR relaxes the specifications of the anti-aliasing filter and allows its integration by just adding external capacitors to the IA's second stage as showed in Fig. 3. The gains of the 1st and 2nd stages of the IA are 8 and 50 V/V respectively, resulting in a total gain of 400 V/V with a cut-off frequency of 15 Hz. The cut-off frequency was selected based on the bandwidth of the signal that will be monitored in this application, blood pressure of small animals.

Table 1 Different options available from suppliers of implantable batteries

Battery	Voltage (V)	Volume (cc)	Capacity (mAh)	Chemistry
Quallion (QL0165)	3.6	30	150	$LiNiCoAlO_2$
Greatbatch (M9107)	2.8	1.4	400[a]	$Li\text{-}I_2$
Eagle Picher (COTENGO)	3.6	1.66	350	$Li/SOCl_2$

[a] Maximum peak current drain <100 μA

2.2.2 Digital communication and RAM organization

Since the MCU has a 16-bit central processing unit (CPU) and the SAR-ADC has a 12-bit resolution, the 4 most significant bits of each stored sample are kept as reserved bits. The MCU's direct memory access (DMA) module uses a transfer channel (DMA1) to send the data from the ADC's buffer to the 8 KB RAM with no CPU intervention [4]. The RAM is organized in 18 pages. Each page includes 217 words of 16 bits, and a data packet consists of 9 of these pages. When a data packet is ready to be transmitted, a second transfer channel of the DMA module (DMA2) sends the data to the serial peripheral interface (SPI)

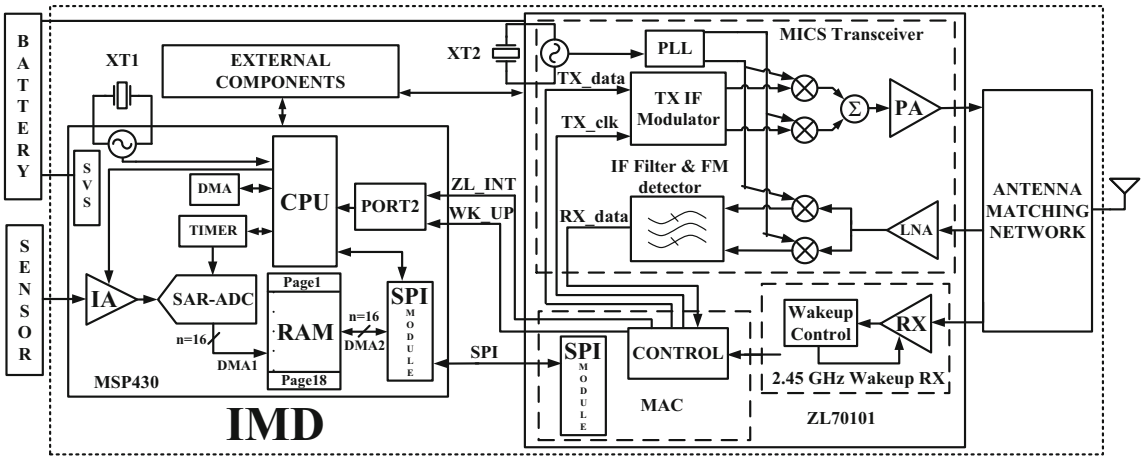

Fig. 2 Detailed block diagram of the IMD unit

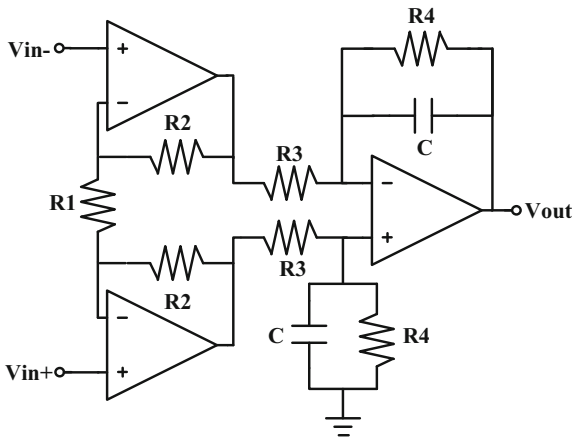

Fig. 3 A three op amp IA with embedded anti-aliasing filter

module. Again, no CPU intervention is needed to transport the information from the RAM to the SPI module, thus allowing reduction of the power consumption. Using the SPI module, the sampled data and control commands are transferred from the MCU and to the transceiver. The transceiver has its own SPI module and receives the 8-bit words sent by the MCU with a data rate of 2 mega samples per second using a shared clock provided by the MCU.

Figure 4 shows a timing diagram of the master device (MCU) while it transmits and receives data. The SPI module uses three pins to operate, a clock (CLK), the slave-input master-output (SIMO) and the slave-output master-input (SOMI). Depending on the clock polarity, SIMO will start transmitting at the rising or falling edge of CLK and SOMI will sample the incoming data at the opposite clock edge [4].

2.2.3 *Wireless transceiver and matching network*

Once in the transceiver, the data is codified and encrypted in the MAC. Then, an intermediate frequency (IF) modulator receives the digital data and a clock stream from the MAC, and converts the data into in-phase and quadrature (I&Q) signals at IF = 450 kHz [5]. The resulting scheme is a four-level frequency shift keying (4FSK) modulation with a maximum effective data rate larger than 200 Kbps [5]. The modulated signals pass through a pair of balanced mixers, fed by I&Q pairs of both IF and local oscillator (LO) signals, for up-conversion to the selected channel in the MICS band. The outputs of the mixers are added and result in a single-sideband signal with suppression on the unwanted opposite sideband. This signal passes through a

Fig. 4 Timming diagram of the SPI link between the MCU and the transceiver

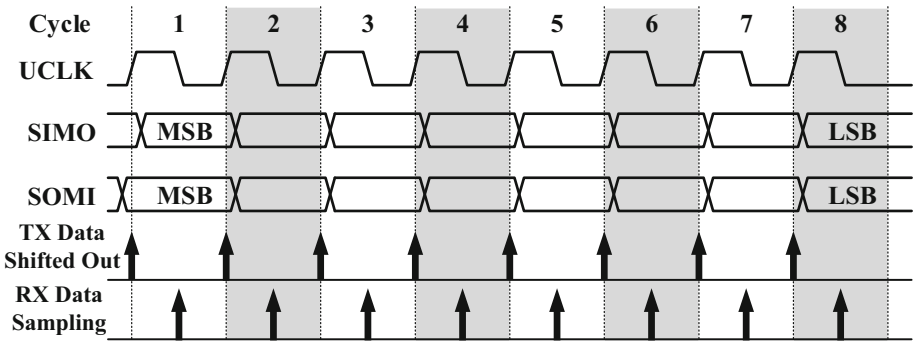

power amplifier (PA) stage which provides a maximum output signal of −3dBm. Finally, the signal goes into an external matching network and is radiated by the antenna.

When the IMD receives information using the MICS band, the signal from the antenna passes through the matching network and then is injected to the on-chip low noise amplifier (LNA). Then, the signal passes over a pair of balanced mixers similar to the ones used in the transmitter. The mixers produce a pair of I&Q signals at IF = 450 kHz [5]. This is followed by an IF Filter and a FM detector which translates the frequency deviations to a time-varying voltage level. The resulting baseband signal is converted to the digital domain by a 2-bit quantizer [5]. The digitized data is sent to the MAC for correlation and clock recovery. Finally, the recovered data is transferred to the MCU using the SPI link described before.

Figure 5 shows the external matching network needed to operate the transceiver in the ISM and MICS bands while using a dual-band antenna. The RF signal received by the antenna goes through a capacitor (C_X) for AC coupling and is followed by an LC tank (C_Y and L_Y) that acts as notch to filter out signals centered at the ISM band. A surface acoustic wave (SAW) filter is used to limit the incoming information to content centered at the MICS band. The SAW filter used in this work is a customized design from Kyocera with a center frequency of 403.5 MHz and bandwidth of 3 MHz [16]. A pi-network (C_{P1}, C_{P2} and L_P) is used to match the impedance of the SAW filter at port 2 (P_2) to the impedance of the antenna while a high-pass LC network (C_{Z1} and L_{Z1}) performs impedance transformation between port 1 (P_1) and the RX/TX MICS band pin of the transceiver. When a wake-up signal (ISM band) is received by the antenna, it is rejected by the notch filter mentioned above and passes through a low-pass LC network (C_{Z2} and L_{Z2}) that conducts impedance transformation between the wake-up pin of the transceiver and the antenna. The values of the matching network components are presented in Table 2.

As mentioned before, the wireless link using the MICS band can be used for data and commands transmission, and it can even work to start communication between the IMD and BS. Nevertheless, using it to periodically listen for the BS's wake-up signals would result in excessive power consumption since the receiver is composed by several power hungry blocks. In order to provide an ultra-low-power wake-up mechanism, the ZL70101 includes a 2.45 GHz receiver using an on/off key (OOK) modulation employing a dedicated frequency band with modest consumption power for the start-up process. By using the OOK scheme there is no need for a local oscillator while the use of a predefined frequency (a channel within the ISM band) for the wireless transmission reduces the complexity of the receiver [5]. On this way the on-chip ultra-low-power receiver is be used instead of the MICS receiver in order to start the IMD operations.

2.3 Base station and GUI

The base station of the ZL70101 application development kit from Microsemi is employed as BS unit in this work. Its design is similar to the IMD in the sense that it is based on the same transceiver and that the employed MCU belongs to the MSP430 family. A block diagram of the BS is presented in Fig. 6. The signal from the IMD is received by a multi-band helical antenna and passes through the matching network and transceiver similarly as explained in the previous subsection. The transceiver receives the data and sends it to the MCU through the SPI module. The MCU then transfers the data to a USB interface chip through a serial non-synchronous link and the aforementioned IC handles the communication with the computer. In the computer, the GUI performs the data processing and stores the received data. Using the GUI, the user can modify the link features such as modulation, data rate and frequency of data collection.

When the GUI receives an instruction from the user, the instruction is transmitted to the MCU via USB and the microcontroller sends it to the transceiver using the SPI bus. To start a transmission, a 2.45 GHz transmitter sends a wake-up signal using a dedicated ISM band transmitter and the IMD replies using the MICS band. Both, the BS and the IMD units, perform a wireless handshaking using the MICS band and finally, the BS unit transmits the instruction to the IMD where it is processed.

3 Control algorithm

3.1 Basics

The selected MCU is designed from the outset for low-power operation. Power optimization is achieved through the use of a range of low-power modes (LPM) supported by a versatile clock system [17]. Figure 7 shows the different MCU operating modes that will be used by the control algorithm along with their corresponding current consumption values for 3 and 2.2 V supply voltages. When the MCU operates in active mode (AM), all the internal clocks and enabled modules are active. On the other hand, while operating in a specific LPM, a selected number of clocks are enabled and only the peripherals driven by the active clocks can be used. For example, during LPM0 the MCU main clock (MCLK) is disabled while the sub-main clock (SMCLK) and the auxiliary clock (ACLK) are active. This allows the operation of high speed peripherals such as SPI and DMA modules with no CPU intervention. Similarly,

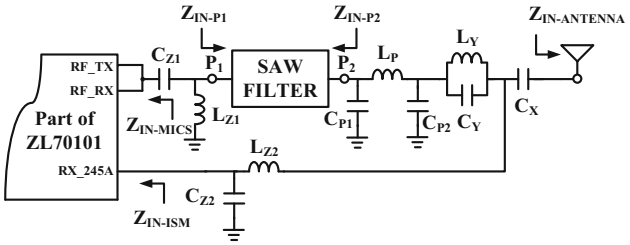

Fig. 5 Dual-band matching network of the IMD

Table 2 Values of the matching network components

Component	Value	Component	Uplink
C_{Z1}	120 pF	C_Y	1.2 pF
L_{Z1}	19 nH	L_Y	2.7 nH
C_{P1}	5.6 pF	C_X	30 pF
C_{P2}	5.6 pF	L_{Z2}	3.3 nH
L_P	18 nH	C_{Z2}	0.75 pF

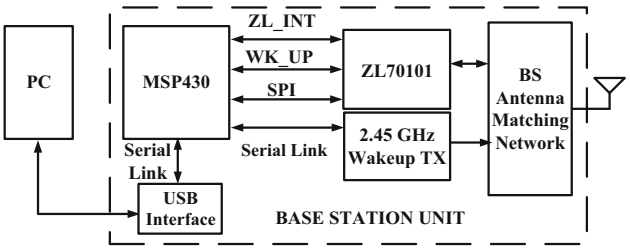

Fig. 6 Block diagram of the base station unit

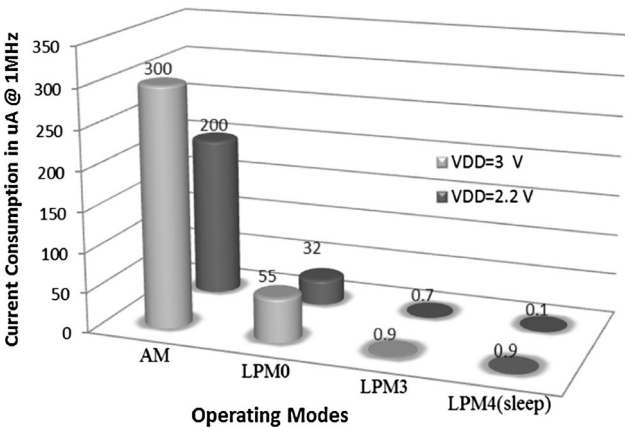

Fig. 7 Different operating modes of the MCU(from datasheet) [17]

when the MCU operates in LPM3, only ACLK is active and the MCU is restricted to use only the peripherals performing low frequency tasks such as the op amps, the SAR-ADC and the timer.

3.2 Proposed low-power-oriented control algorithm

The goal of the algorithm is to switch the MCU between AM, LPM0, and LPM3 using interrupts [18]. Interrupts are generated by hardware or software to respond to an urgent event by executing an interrupt service routine (ISR) [17]. The principle of operation is the following: when the MCU is in a LPM, an interrupt automatically switches the device to AM where the ISR finds the interrupt source and sets a flag to inform the main program what task needs to be performed. The MCU returns to the main program, serves the ISR and goes back into a LPM. This process is repeated each time a new interrupt is asserted.

A basic flow chart of the proposed control algorithm is presented in Fig. 8 where the interrupt sources are the DMA, the timer and the transceiver chip (TX/RX interrupt). The main program initializes the MCU (routine INT_MCU) and sends the MCU to LPM3 where it waits for a wake-up signal to continue. The INIT_MCU routine consists of the following subroutines: *Init_McIO*, selects the ports that will be used as digital/analog inputs/outputs and enables the external interrupt to be used to assert the TX/RX interrupt. *InitAnalogPeripherals*, initializes the analog peripherals that are used by the IMD: SAR-ADC and the three op amps that compose the IA. This subroutine also sets the control registers of the timer that will be in charge of triggering the ADC and the DMA channels that will transfer information between the RAM and different peripherals. *SPIInit*, initializes the SPI peripheral by setting the clock frequency/polarity, the port used for the communication and the size of the word that will be transmitted. Finally, *MicsInit* initializes the transceiver by sending command to set its control registers.

When the wake-up signal is received by the transceiver, the TX/RX interrupt is asserted and the TX/RX_ISR enables the timer and the other interrupts. Then it switches the MCU to LPM3 and waits for the next interrupt to be asserted. The next interrupt to be asserted is from the timer used to start ADC conversions. When this interrupt is asserted, the TIMER_ISR sets a flag and IM_PROC enables the ADC. Then MCU goes into LPM0, the ADC sample is sent to the RAM through the DMA1 and the

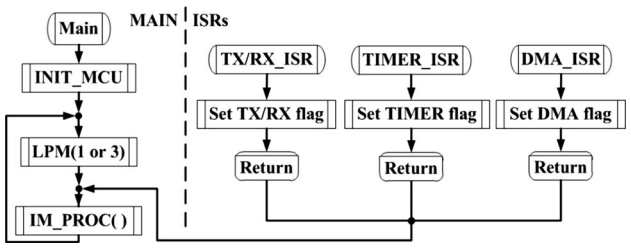

Fig. 8 Basic flow chart of the implemented algorithm

MCU returns to LPM3. This continues until one RAM page (217 samples) has been filled with data and the DMA interrupt is asserted. Then, the DMA_ISR sets a flag to let IM_PROC know that one memory page has been written and the DMA1 channel destination addresses is updated in order to write the incoming data into the following memory page.

When a data packet (9 pages) is ready for transmission, IM_PROC enables the SPI module to communicate the MCU with the transceiver and the DMA2 channel sends information from the RAM to the SPI output buffer. When one RAM page has been transmitted to the SPI output buffer the DMA interrupt is asserted again but this time due to the DMA2 channel. The DMA_ISR sets a flag and IM_PROC updates the source address of the DMA2 channel to start reading the next memory page. This happens until the complete data packet is transmitted. Since the RAM can store up to two data packets, while one is transmitted to the BS unit, the other is used to store new physiological samples. This sequence occurs continuously or periodically depending on the settings defined by the user. More details on this regard will be provided in the next section.

The remaining TX/RX interrupt sources are the transmit/receive RF buffers, the SPI bus, a link monitoring register that tracks the communication between the IMD and the BS unit, and another control register that indicates when an instruction command has been completed. When they are asserted, the routine IM_PROC uses the SPI module to read the interrupt vector of the transceiver. In order to serve the different interrupts, the MCU sends instruction commands to the transceiver to perform tasks such as restart the wireless link, read/write data on the TX/RX buffers, or clear the required interrupt vector bit.

As a result of the implemented algorithm, the MCU remains in LPM3 most of the time, waiting for the next interrupt to be asserted and, hence, the power consumption of the IMD is optimized.

4 Power analysis

The IMD power consumption varies with time depending on the task being performed. By knowing the power consumption and the duration of each task, the IMD average current (I_{AV}) can be computed and its lifetime can be estimated.

4.1 Continuous sampling mode

Figure 9 shows a timing diagram of the tasks performed by the IMD while sampling a blood pressure signal with a frequency of 5 Hz. This frequency is used since several physiological signals fall below this bandwidth [14]. In this figure, t_T is total time needed to collect and transmit a data packet (nine pages of 217 words), t_P is the time needed to write a data packet inside the RAM, t_{TX} is the time required for the RF transmitter to submit the data stored in the RAM to the BS, t_{AS} is the time between adjacent samples, t_C is the ADC conversion time (13 cycles of the 32.758 kHz clock that drives the ADC [4]) and t_{AQ} ($1/f_S$) is the acquisition time given by $t_{AS} + t_C$. For the transceiver with a data rate of 200 Kbps and 16-bit resolution for each sample, the IMD can transmit 12.5 kilo samples per second. Having this transmission rate and an ADC's oversampling rate of 20 ($f_S = 100$ Hz), the timing parameters in Fig. 9 have the following values: $t_C = 13/32{,}758 \approx 0.4$ ms, $t_{AS} = (1/f_S) - t_C = 10 - 0.4$ ms $= 9.6$ ms, $t_P = 9 \times 217 \times t_{AQ} = 19.44$ s, $t_{TX} = 9 \times 217/12.5$ K $= 0.156$ s and the total time is $t_T = t_P + t_{TX} = 19.596$ s. From these numbers, it is possible to observe that the IMD remains in RF transmission mode around 0.8 % of the total time to collect and transmit a data packet. The scenario where the IMD has the previous timing parameters and sends information to the base station without interruption is defined as continuous sampling mode (CSM). The following equation is used to calculate the average current consumption (I_{AVC}) of the IMD in CSM:

$$I_{AVC} = \frac{217 \times 9(t_C \times I_C + t_{AS} \times I_{AS}) + t_{TX} \times I_{TX}}{t_T}, \qquad (3)$$

where I_C is the current consumption during t_C, I_{AS} is the current consumption during t_{AS} and I_{TX} is the current consumption during t_{TX} with values of 0.65, 0.5 and 6 mA respectively. The current values are taken from [4] and [5]. Using (3), it is possible to predict an I_{AVC} around 0.549 mA. Moreover, based on the current capacity of the selected battery (350 mAh [8]), the estimated lifetime of the IMD in CSM can be obtained using the ratio of the battery capacity and I_{AVC}, resulting in approximately 26.5 days. This battery was chosen as the power source due to its small size (6.6 mm × 16.5 mm × 15.2 mm = 1.66 cc, 4.6 g) and large current capability. The time and current values presented in this subsection are summarized in Table 3.

4.2 Periodic sample mode

Since the average current is inversely proportional to the lifetime, increasing the lifetime of the IMD can be achieved by decreasing I_{AV}. In order to extend the lifetime, the IMD average current consumption can be reduced using a variation of the CSM where only a fixed number of data packets is collected in a given period of time. This is done in the following way: the user defines the number of packages to be collected using the GUI, the IMD operates continuously until the last data packed is submitted to the BS and finally, the MCU switches to sleep mode (LPM4)

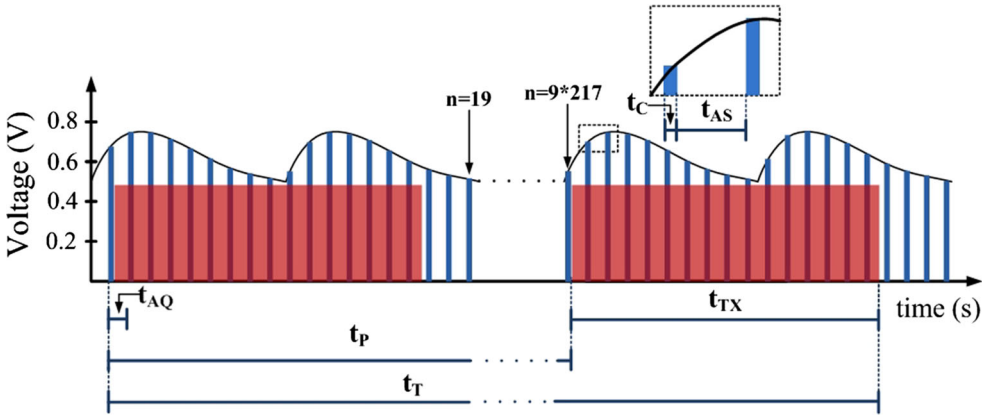

Fig. 9 Timming diagram of the IMD sampling a biological signal in CSM

Table 3 Summary of the time and current values for different IMD tasks

Parameter	Time (ms)	Parameter	Current (mA)
t_C	0.4	I_C	0.65
t_{AS}	9.6	I_{AS}	0.5
t_{TX}	156	I_{TX}	6
t_T	19,596	I_{AVC}	0.549

until a new set of data is required. During sleep mode the microcontroller turns off all the peripherals and waits for a new wake-up signal. This variation of CSM is defined as periodic sampling mode (PSM). Figure 10 shows the timing diagram of the IMD current in PSM, where t_{AQ}, t_P and t_T refer to the parameters presented in Fig. 9, t_{OFF} is the time in which the circuit remains in sleep mode and I is the current consumption of the IMD depending on the task being performed. Finally, t_{DS} is defined by $t_{ON} + t_{OFF}$ and the frequency of data collection (f_{DS}) is the inverse of t_{DS}. The following equation is used to compute the average current during PSM:

$$I_{ACP} = \frac{t_T \times I_{AVC} + t_{OFF} \times I_{OFF}}{t_{DS}}, \quad (4)$$

where $I_{OFF} = 0.9$ μA is the current consumption of the MCU during t_{OFF} [4]. Figure 11 shows a prediction of the lifetime in months and the number of data packets transmitted from the IMD to the BS during 1 day. This plot is based on Eqs. (3) and (4), and the timing parameters and battery capacity presented before. A linear relationship between the ratio of t_{OFF} and t_T and the lifetime of the

IMD is observed while the amount of collected data decreases and tends to saturate. For example, in points A and B the ratios are 1 and 10 resulting on 1.7 and 9.2 months of lifetime with 2,212 and 403 data packets per day respectively. This plot can be used to choose the t_{OFF}/t_T ratio that would fit better with the designer's needs.

5 Measurements and results

5.1 IMD prototype implementation

A prototype of the IMD has been implemented in order to demonstrate the operation of the low-power-oriented control algorithm and to corroborate the results obtained from the lifetime estimation presented in the previous section.

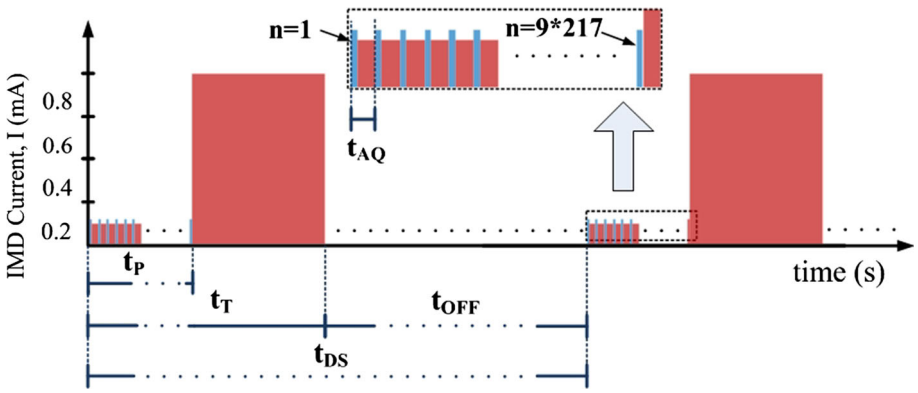

Fig. 10 Timming diagram of the IMD operating in periodic sampling mode (PSM)

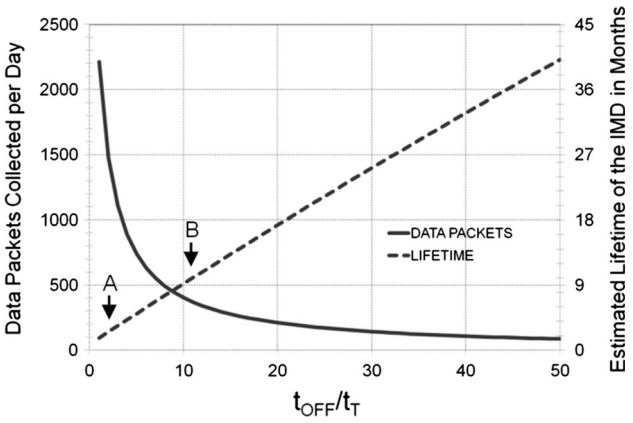

Fig. 11 Lifetime and data packets per day versus t_{OFF}/t_T for a 350 mAh battery

The fabricated IMD printed circuit board (PCB) is presented in Fig. 12. The 2-layer PCB has a total area of 50.7 cm^2 (7.12 cm × 7.12 cm) and was fabricated with a 0.062 FR4 substrate. The dual-band printed loop antenna (PLA) showed on the left side of the picture was provided by Microsemi and accounts for body losses allowing the emulation of real conditions over free air.

5.1.1 Debug and testing for measurements under controlled conditions

The implemented PCB features different debug and testing capabilities in order to allow measurements emulating implantation of the prototype before fabricating the final IMD unit with actual implantable dimensions. The main debug resources include a J-TAG receptacle that allows upgrades on the MCU's firmware; a variable R1 resistor used to modify the IA total gain; a set of LEDs used to monitor the link indicating the MICS transmitter or receiver operation, the status of the connection between IMD and BS and if a wake up signal has been received by the IMD; a BNC connector to emulate different biological signals using an function/arbitrary waveform generator (FAWG) and push buttons to reset or start manually the IMD. For testing capabilities, the IMD includes test points to monitor different key signals from the IA (gains of the 1st and 2nd stages), MCU (timer output, DAC output, crystal oscillator XT1, etc.), SPI link (CLK, SIMO, SOMI and CS) and the TX/RX (programmable outputs, voltage references, crystal oscillator XT2, etc.). The IMD prototype also includes a set of jumpers to manually enable/disable MCU modules and LEDs in order to measure the current consumption of the IMD in different nodes and with the MCU operating in different power modes.

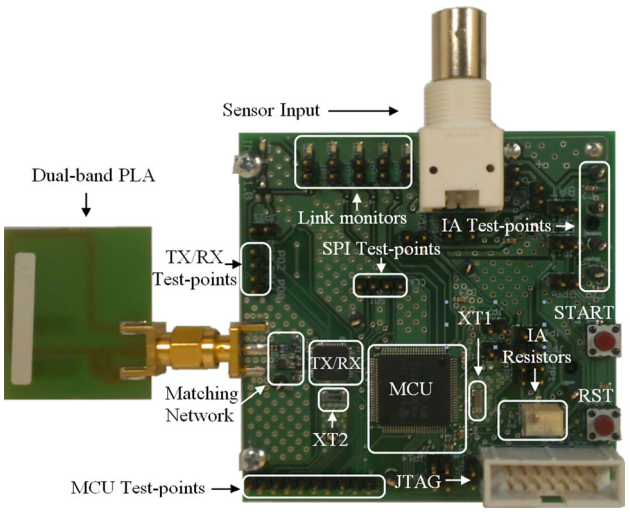

Fig. 12 Fabricated implantable medical device prototype board

The fabricated prototype also includes bypass capacitors to filter out high frequency noise and to ensure good load regulation. Besides this, the MCU and Tx/Rx chips contain internal LDOs to provide the required voltage for the different sections of the circuits. The capacitors used for the battery and for the LDOs inside the MCU and Tx/Rx are external and have low ESR in order to reduce any ripple originated by the battery voltage during low-to-high current transitions such as the change from sleep mode to RF transmission.

5.1.2 Board optimization

The highlighted areas in Fig. 12 include the aforementioned MCU and TX/RX along with their external components: bypass capacitors, crystals 1 and 2, IA resistors/capacitors and the matching network elements. The presented prototype was fabricated for testing purposes. Nevertheless, the IMD area can be optimized by removing the variable R1 resistor along with all the debug/testing hardware (also highlighted). These modifications would result in an effective board area of 6.5 cm^2 (12.8 % of the original size). Furthermore, if each IC is placed on the top and bottom sides of a PCB, an IMD effective area of 2.7 cm^2 can be achieved.

5.2 Link analysis

This subsection discusses the main factors to be considered while designing a wireless link for implantable applications. The following expression [19] is a simple link budget equation that can be used for typical uplink/downlink calculations:

$$P_{RX}|_{dBm} = P_{TX}|_{dBm} + G_{TX}|_{dB} - L_T|_{dB} + G_{RX}|_{dB}, \quad (5)$$

where $P_{RX}|_{dBm}$ is the power available at the receiver input terminals, $P_{TX}|_{dBm}$ is the signal power available from the transmitter output terminal, $G_{TX}|_{dB}$ is the gain of the

transmitter antenna including cable and matching losses, $L_T|_{dB}$ represents the total of losses between the transmitter output and the receiver input and $G_{RX}|_{dB}$ is the gain of the receiver antenna including only matching losses. Nevertheless, this is not a typical application and some modifications should be considered in order to have accurate results.

First, it is critical to take into account that the propagation path of the presented link happens through two different media: free air and the subjects' body. The total loss between the IMD antenna input and the outside of the subjects' body, including matching network and IMD package losses is between 40 and 45 dB [6]. Also, the MICS standard requires the antenna gain and the propagation path loss within the body to be combined together when calculating the effective radiated power (ERP) of the IMD transmitter [20]. Therefore, the ERP can be defined as:

$$P_{TX(ERP)}|_{dBm} = P_{TX}|_{dBm} + G_{TX}|_{dB} \quad (6)$$

Moreover, the BS and IMD output power levels are restricted to a maximum ERP of −16 dBm in a reference bandwidth of 300 kHz to prevent interference with meteorological aids [6]. Using (6) and having a BS antenna gain of −5 dBi including losses, the maximum power transmitted by the BS unit is −11 dBm. For the IMD, the transmitter is programmed to have an output power of −3 dBm and the antenna gain including body and matching losses is −42 dB, resulting in an ERP of −45 dBm. Therefore, since the in-body losses are much more significant than any cable or matching loss at the BS unit, the power transmitted by the IMD is higher than the one transmitted by the BS unit.

The total loss between the transmitter and the receiver $L_T|_{dB}$ consists of the free-space path loss $A_{FSL}|_{dB}$ and a "fading margin" $A_{FADE}|_{dB}$ of 5 dB is added to allow for destructive interference. The free-space path loss depends on the wavelength and the distances as shown in the following equation [19]:

$$A_{FSL}|_{dB} = 20Log\left(\frac{4\pi d}{l}\right) \quad (7)$$

Using Eqs. (6) and (7), the original link budget equation can be defined as:

$$P_{RX}|_{dBm} = P_{TX(ERP)}|_{dBm} - A_{FSL}|_{dB} - A_{FADE}|_{dB} + G_{RX}|_{dB} \quad (8)$$

The minimum detectable signal (MDS) is defined as the minimum $P_{RX}|_{dBm}$ level present at the receiver to perform a successful transmission. This computing MDS using the following equation [19]:

$$MDS|_{dBm} = NF|_{dB} + 10Log(kTB)|_{dB} + 30 + SNR_{MIN}|_{dB}, \quad (9)$$

where $NF|_{dB}$ is the noise figure of the receiver, k is the Boltzmann constant, T is the temperature in Kelvin degrees, B is the bandwidth of interest (B = 300 kHz), 30 is added to convert the integrated noise floor to dBm and $SNR_{MIN}|_{dB}$ is the minimum signal to noise ratio (SNR) required for a maximum allowed bit error ratio (BER). The NF of the IMD and the BS units operating with a data rate of 200 Kbps using 2FSK modulation in the downlink (BS to IMD) and 400 Kbps with 2FSK in the uplink (IMD to BS) are 5 and 9 dB with $SNR_{MIN}|_{dB}$ values of 14 and 17 dB respectively [21]. Using (9) the MDS levels of the BS and IMD units are found to be −90 and −99 dBm (40.2 and 14 μV_{rms} with an effective resistance of 1,620Ω), respectively.

5.3 Measurement setup and experimental results

The implantable WMS measurement setup is shown in Fig. 13. In this test, a 5 Hz blood pressure signal is emulated using the Agilent 33,220 A FAWG with a peak-to-peak amplitude of about 1 mV and a DC offset of 0.5 mV. This signal is injected to the IMD where it is amplified, converted to the digital domain and transmitted to the BS unit through the RF channel using the MICS band. The BS unit receives the wireless data and sends it to a computer via USB. In the computer, the GUI stores the data and performs post-processing operations.

In order to verify the operation of the system the IMD and FAWG were placed at a fixed location while the BS unit was moved away from the device to perform transmission measurements in the line of sight. Measurements were taken at each step of 10 cm. The maximum distance of the wireless communication link achieved in the MICS band is 2.1 m in the line of sight. This distance includes

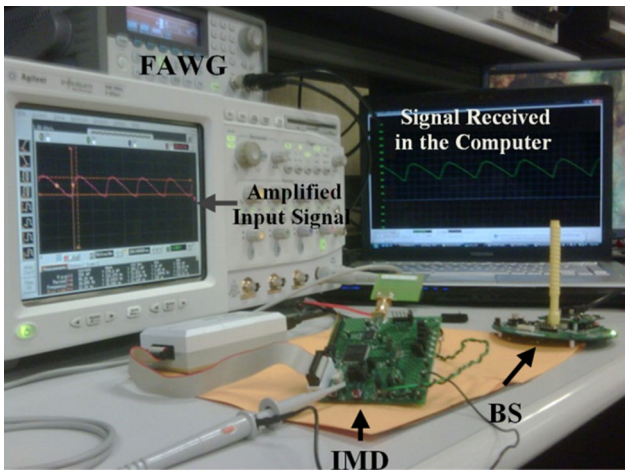

Fig. 13 Measurement setup for measurements emulating implantation of the IMD prototype

30 cm more than the design specification (1.8 m) in order to account for extra losses including packaging losses. Table 4 presents the link measurement results for this distance with data rate of 200 Kbps and using the channel located at 403.5 MHz. $P_{RX}|_{dBm}$ and $P_{TX}|_{dBm}$ were taken from the transceiver's measurement registers and the other parameters were calculated using (5)–(8). Notice that $P_{TX(ERP)}|_{dBm}$ for the uplink is smaller than the value computed in the previous section (−45 dBm). To understand the reason of this difference, let us use Eq. (6), the measured ERP (−49 dBm) and $P_{TX}|_{dBm} = -3$ dBm, to compute the antenna gain minus losses $G_{TX}|_{dB}$ in the uplink ($G_{RX}|_{dB}$ for the downlink). This value results in a value of −46 dB, meaning that there are extra losses in the dual-band PLA in comparison with the estimated value. This discrepancy can be due to variations on the matching network components or the length of the PCB traces used to connect the antenna. Nevertheless, the results are still close to the values predicted on the link budget calculations and therefore, the presented method can be used as a start point for designing a WMS for implantable applications.

Figure 14 shows a comparison between the amplified signal at the input of the ADC (in the IMD) and the data received at the BS unit for a distance of 2.1 m. Notice that the transmission delay (t_{TX}) is not taken into account since the purpose of this figure is to show the signals in a direct comparison. The sampling frequency of the ADC was 300 Hz and the frequency of the input signal was 10 Hz.

Figures 15 and 16 show the measured return loss of the IMD's dual-band-PLA and the BS's multi-band helical antenna, respectively. Both antennas were provided by Microsemi and operate in the ISM and MICS bands, as observed on the figures, allowing the use of the ultra-low-power wake-up mechanism described in Sect. 2.

Since the purpose of this work is to provide a design methodology and proof of concept of the proposed low-power oriented algorithm, a 3 V Li/MnO_2 battery (Panasonic CR2354) is used as power supply. Nevertheless, in order to verify that the results are valid for the proposed 350 mAh reference battery, the IMD current consumption for using a variable DC power supply with voltages from 4 V down to 1.8 V was measured. The results showed

Table 4 Link budget parameters with d = 2.1 m

Parameter	Downlink	Uplink
$P_{TX(ERP)}\|_{dBm}$	−16	−49
$A_{FSL}\|_{dB}$	31	31
$A_{FADE}\|_{dB}$	5	5
$G_{RX}\|_{dB}$	−46	−5
$P_{RX}\|_{dBm}$	−98	−90

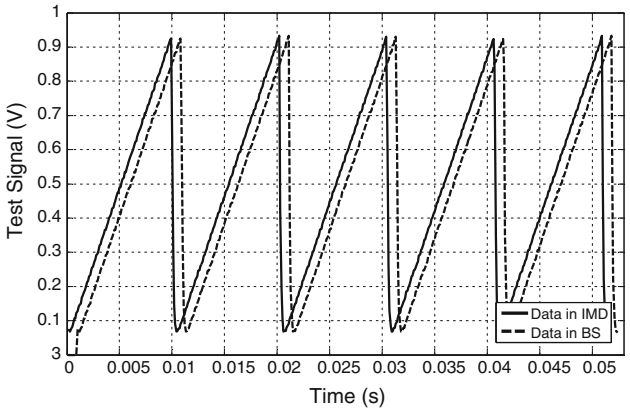

Fig. 14 Signal at the ADC input versus data received at the BS, d = 2.1 m

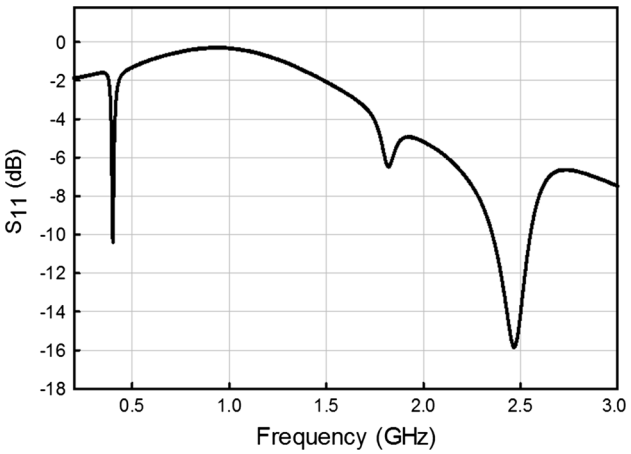

Fig. 15 Measured S11 of the dual-band PLA used in the IMD

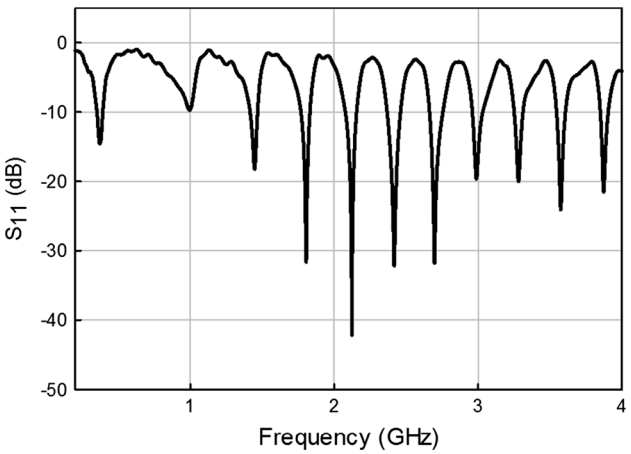

Fig. 16 Measured S11 of the multi-band helical antenna used in the BS

small variations (∼10μA) on the average current consumption. This is explained knowing that the internal power management systems of the MCU and Tx/Rx deliver

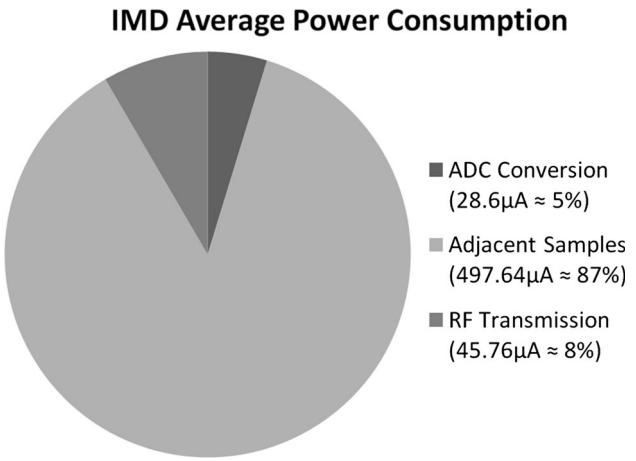

Fig. 17 Pie chart showing the measured average power consumption of the IMD in while performing different tasks

a fixed current independently of the input voltage as a result of using dedicated linear voltage regulators. The found that a 3 V supply voltage is the minimum value to fulfill the wireless link range spec required for this application (1.8 m), with 0.3 m as safe margin, resulting in the reported total 2.1 m.

Finally, power measurements showed an average current value of $I_{AVC} = 0.572$ mA for a 3 V power supply, corresponding closely to the calculations performed in Sect. 4. The average current consumption of the IMD while performing different tasks is shown in Fig. 17. Using this I_{AVC}, the IMD prototype lifetime is 1.7 months operating in continuous mode with a projected 2.7 cm^2 area. This can be compared with 1.5 months and approximately 1.9 cm^2 offered by the commercial implantable blood pressure monitor for small animals from [22].

6 Conclusion

This paper has presented the design, implementation and testing of a WMS prototype for implantable applications meeting FCC standards. Special attention was placed on the realization of the implantable unit in order to obtain the best trade-off between size, cost and power. A thorough explanation of the signal path, starting as an analog waveform from the sensor and reaching the PC as digital information has been presented.

The comprehensive power analysis presented in Sect. 4 and the link budget study from Sect. 5 provided results close to the measurements performed while emulating the implantation of the IMD. Therefore, a similar methodology can be used to predict the lifetime of generic monitory units (invasive or non-invasive) and to make a realistic link analysis from the very beginning of the design stage.

The proof-of-concept IMD prototype includes several testing/debug capabilities and is designed to allow the integration of different sensors to monitor other biological parameters with minimal modifications. Moreover, suggestions for the optimization of the presented IMD and the implementation of the final implantable unit have been discussed.

Acknowledgments The authors would like to thank the Mexican National Council for Science and Technology (CONACYT) for their partial funding and support.

References

1. Choi, J. H., & Kim, D. K. (2011). Health-care devices using radio frequency technology. In K. Iniewski (Ed.), *CMOS biomicrosystems* (pp. 93–117). New York: Wiley.
2. Gaxiola-Sosa, J. E., Mohsin, N., Palliyali, J. A., Tafreshi, R., & Entesari, K. (2014). A portable 12-lead ECG wireless medical system for continuous cardiac-activity monitoring. In *2014 2nd middle east conference on, biomedical engineering (MECBME)*, Doha, Qatar.
3. Gerrish, P., Herrmann, E., Tyler, L., & Walsh, K. (2005). Challenges and constraints in designing implantable medical ICs. *IEEE Transactions on Device and Materials Reliability, 5*, 435–444.
4. Texas-Instruments. (2007). MSP430x4xx Family User's Guide. In *SLAU056G* [Revised 2013].
5. Bradley, P. D. (2006). An ultra low power, high performance Medical Implant Communication System (MICS) transceiver for implantable devices. In *IEEE Conference* in *Biomedical Circuits and Systems 2006, (BioCAS)* (pp. 158–161).
6. FCC. (November 2002). FCC rules and regulations 47 CFR part 95, subparts E (95.601–95.673) and I (95.1201–95.1219). Personal Radio Services, Washington, DC.
7. Holmes, C. F. & Owens, B. B. (2006). Batteries for implantable biomedical applications. In *Wiley encyclopedia of biomedical engineering*. Hoboken: John Wiley & Sons, Inc.
8. Eagle-Picher-Medical-Power. (2009). Implantable medical batteries catalog, Joplin, MO.
9. Pallas-Areny, R., & Webster, J. G. (1993). AC instrumentation amplifier for bioimpedance measurements. *IEEE Transactions on Biomedical Engineering, 40*, 830–833.
10. Chih-Jen, Y., Wen-Yaw, C., & Mely Chen, C. (2004). Micropower low-offset instrumentation amplifier IC design for biomedical system applications. *IEEE Transactions on Circuits and Systems I: Regular Papers, 51*, 691–699.
11. Smither, M. A., Pugh, D. R., & Woolard, L. M. (1977). C.M.R.R. analysis of the 3-op-amp instrumentation amplifier. *Electronics Letters, 13*, 594.
12. Schaumann, R., & Van Valkenburg, M. E. (2001). *Design of analog filters*. New York: Oxford University Press.
13. Maloberti, F. (2008). *Data converters*. Dordrecht: Springer.
14. Webster, J. G. (1998). *Medical instrumentation: Application and design* (3rd ed.). New York: Wiley.
15. Yazicioglu, R. F., Van Hoof, C., & Puers, R. (2009). *Biopotential readout circuits for portable acquisition systems*. New York: Springer.
16. Kyocera Corporation. (2008). RF SAW filter SF16-043C5UU01 datasheet.
17. Davies, J. (2008). *MSP430 microcontroller basics*. Oxford: Elservier.

18. Texas-Instruments. (2007). MSP430 software coding techniques. In *Appl. Note SLAA294A*.
19. Gu, Q. (2005). *RF system design of transceivers for wireless communications*. New York: Springer.
20. International Telecommunication Union. (1998). *Recomendation ITU-R SA.1346*. Geneva, Switzerland: Headquarters.
21. Microsemi-Corporation. (2012). Medical implantable RF transceiver ZL70101, datasheet.
22. Data-Science-International. (2012). PAC-12 PhysioTel Transmitter, St. Paul, MN.

Jesus Efrain Gaxiola-Sosa was born in Merida, Yucatan, Mexico in 1985. He received the B.S. degree in Electrical Engineering with high honors from the Merida Institute of Technology, Merida, Mexico, in 2008 and the Ph.D. degree in Electrical Engineering from Texas A&M University, College Station, TX, in 2014. He participated as system engineer intern with Texas Instruments (Power Management Group) in 2010 and as IC design inter with Biotronik in 2012, working on DC/DC converters design and medical implantable analog circuit design respectively. In 2014, he joined Silicon Labs, Austin, Texas, as Applications Engineer. Dr. Gaxiola-Sosa received a full Ph.D. scholarship from the Mexican National Council for Science and Technology (CONACYT) and the Youth State Award from the State of Yucatan (Mexico) in 2012. His research interests include ultra-low power analog front-ends for biopotential signals, implantable medical devices and RF/baseband circuitry for RF receivers.

Kamran Entesari (S'03–M'06) received the B.S. degree in Electrical Engineering from the Sharif University of Technology, Tehran, Iran, in 1995, the M.S. degree in Electrical Engineering from Tehran Polytechnic University, Tehran, Iran, in 1999, and the Ph.D. degree from The University of Michigan at Ann Arbor, in 2005. In 2006, he joined the Department of Electrical and Computer Engineering, Texas A&M University, College Station, where he is currently an Associate Professor. His research interests include microwave chemical/biochemical sensing for lab-on-chip applications, RF/microwave/mm-wave integrated circuits and systems, reconfigurable RF/microwave antennas and filters, medical electronics and RF MEMS. Dr. Entesari was the recipient of the 2011 National Science Foundation (NSF) CAREER Award. He was the co-recipient of the 2009 Semiconductor Research Corporation (SRC) Design Contest Second Project Award for his work on dual-band millimeter-wave receivers on silicon.